

On the Non-Identifiability of Steering Vectors in Large Language Models

Sohan Venkatesh* Ashish Mahendran Kurapath
Manipal Institute of Technology Bengaluru

Abstract

Activation steering methods are widely used to control large language model (LLM) behavior and are often interpreted as revealing meaningful internal representations. This interpretation assumes steering directions are identifiable and uniquely recoverable from input–output behavior. We show that, under white-box single-layer access, steering vectors are fundamentally non-identifiable due to large equivalence classes of behaviorally indistinguishable interventions. Empirically, we show that orthogonal perturbations achieve near-equivalent efficacy with negligible effect sizes across multiple models and traits. Critically, we show that the non-identifiability is a robust geometric property that persists across diverse prompt distributions. These findings reveal fundamental interpretability limits and highlight the need for structural constraints beyond behavioral testing to enable reliable alignment interventions.¹

1 Introduction

Persona vector steering (Chen et al., 2025) has emerged as a popular technique for controlling the behavior of large language models by adding learned directional vectors to intermediate activations. This line of work is closely connected to broader efforts in representation engineering (Zou et al., 2023) and activation editing (Rimsky et al., 2024; Turner et al., 2023), where linear directions in activation space are used to modulate model behavior along semantic axes (Elhage et al., 2022; Turner et al., 2024).

Despite growing adoption in interpretability and alignment research, the theoretical foundations of persona steering remain poorly understood. Most existing methods implicitly assume that extracted steering vectors correspond to meaningful,

uniquely determined latent factors and that these factors can be directly manipulated to achieve reliable control. However, classical results in latent variable modeling and causal inference show that such assumptions are often unjustified without additional structural constraints (Hyvärinen and Pajunen, 1999; Shimizu et al., 2006; Schölkopf et al., 2021; Locatello et al., 2019).

This raises a fundamental question: *when does representational alignment afford reliable behavioral control?* Understanding identifiability is critical for several reasons. First, it determines when persona vectors provide principled causal interventions versus merely heuristic control that exploits one of many behaviorally equivalent directions. Second, it clarifies when claims that a specific vector “represents” a semantic concept are scientifically well-grounded rather than artifacts of measurement and projection (Elazar et al., 2021; Marks and Tegmark, 2023). Third, it reveals when steering directions may rely on fragile correlations that fail under distribution shift, model updates or adversarial prompting. Finally, identifiability theory clarifies which experimental protocols provide meaningful evidence for causal interpretation of interventions on internal activations (Schölkopf et al., 2021; Ahuja et al., 2022).

We make three contributions. First, we provide a formal identifiability analysis of persona vector steering, proving that under white-box single-layer access, persona vectors are fundamentally non-identifiable: infinitely many geometrically distinct directions induce identical observable behavior via null-space ambiguity. Second, we empirically demonstrate that extracted steering vectors contain substantial non-identifiable components, with orthogonal perturbations achieving 95–100% of the original steering efficacy across multiple models and traits. Third, we validate through multi-environment experiments that this equivalence persists under distribution shift, confirming

*Correspondence: soh.venkatesh@gmail.com

¹Code: <https://github.com/sohv/non-identifiability>

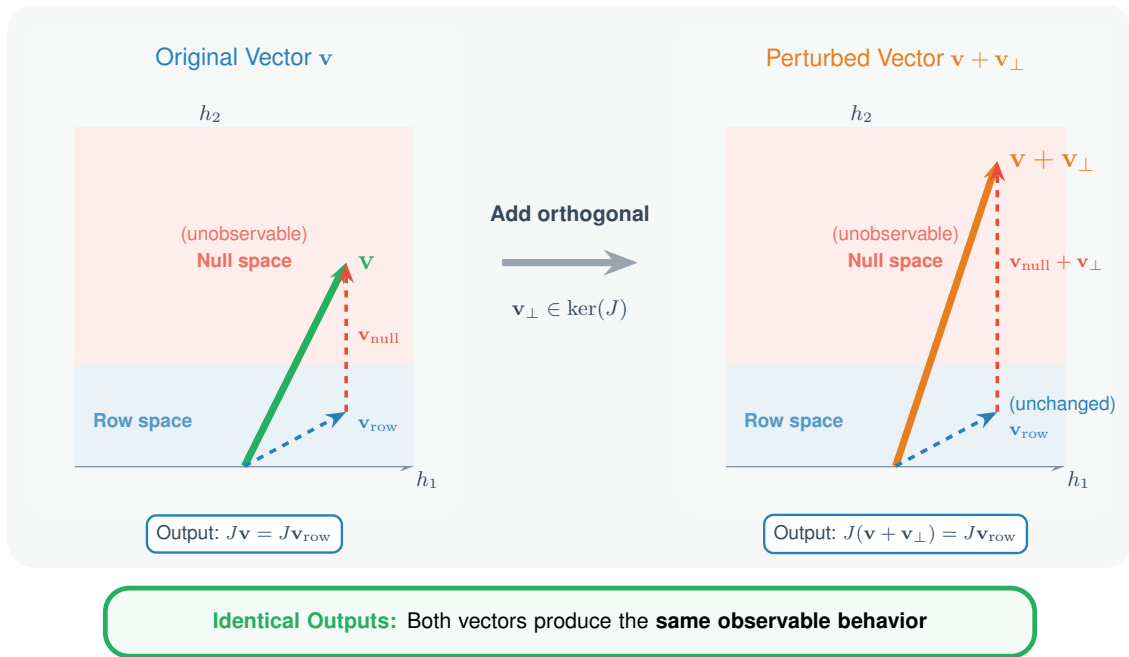


Figure 1: **Geometric illustration of steering vector non-identifiability.** Two geometrically distinct vectors, the original steering vector v (left) and a perturbed version $v + v_{\perp}$ where $v_{\perp} \in \ker(J)$ (right), produce identical observable outputs. The null-space component (red, unobservable region) can be arbitrarily modified without changing outputs, demonstrating the existence of large equivalence classes of behaviorally indistinguishable steering directions.

non-identifiability is a robust geometric property rather than an artifact of limited prompt diversity. These results clarify when alignment methods can be trusted and which structural assumptions are required for reliable control.

2 Related Work

Our work formalizes persona steering² as a latent variable identification problem, bridging causal representation learning, activation editing in LLMs and mechanistic interpretability.

Causal and latent variable identifiability. Classical results show that latent variable models are non-identifiable without structural assumptions (Hyvärinen and Pajunen, 1999; Shimizu et al., 2006; Kruskal, 1977). Recent work in causal representation learning extends these ideas to deep learning settings (Schölkopf et al., 2021; Ahuja et al., 2022; Locatello et al., 2019), establishing conditions under which latent factors can be recovered from high-dimensional observations.

Probing and representation learning. Work on

²We use *persona vectors* and *steering vectors* interchangeably to refer to directional vectors added to model activations to modulate semantic or behavioral attributes (Chen et al., 2025).

probing classifiers (Pimentel et al., 2020; Ravfogel et al., 2020; Elazar et al., 2021) shows that linear directions can succeed for reasons unrelated to target information. The linear representation hypothesis (Park et al., 2023; Elhage et al., 2022) suggests concepts correspond to directions in activation space but lacks identifiability guarantees.

Activation editing in LLMs. Methods such as representation engineering (Zou et al., 2023), contrastive activation addition (Rimsky et al., 2024; Turner et al., 2024) and activation patching (Meng et al., 2022) manipulate model internals but do not address whether control directions are uniquely determined. Work on neural network symmetries (Entezari et al., 2021; Dinh et al., 2017) motivates our null-space analysis.

Robustness and invariant representations. Work on distribution shift and domain adaptation (Rabanser et al., 2019; Lipton et al., 2018) establishes that learned representations often exploit spurious correlations. Methods for learning invariant representations (Arjovsky et al., 2019; Krueger et al., 2021) aim to extract features stable across domains. Recent work on multi-environment causal representation learning (Ahuja et al., 2022;

Von Kügelgen et al., 2021; Rojas-Carulla et al., 2018) proves that diverse training environments enable identification of causal factors under structural assumptions.

Mechanistic interpretability. Work on mechanistic interpretability (Olsson et al., 2022; Elhage et al., 2021; Nanda et al., 2023) studies circuits and features in transformers, often assuming the existence of interpretable directions without formalizing identifiability constraints. Our theoretical analysis clarifies when such directions are well-defined.

3 Problem Setup

3.1 Formal Model

Consider a pre-trained transformer language model f_θ with L layers. For a given input prompt x (tokenized as x_1, \dots, x_T), let $h_\ell(x) \in \mathbb{R}^d$ denote the hidden representation at layer ℓ and position T (typically the final token position for autoregressive generation).

Latent persona variable. We assume there exists an underlying latent variable $z \in \mathcal{Z}$ representing a semantic attribute or "persona" (e.g., formality, political stance, truthfulness).

Steering intervention. A steering vector $v \in \mathbb{R}^d$ is applied as:

$$\tilde{h}_\ell(x) = h_\ell(x) + \alpha v \quad (1)$$

where $\alpha \in \mathbb{R}$ is the steering strength. The modified representation \tilde{h}_ℓ is fed forward through subsequent layers to produce output logits $o(x, v, \alpha)$ over the vocabulary.

Generative model. We posit that the true data-generating process involves:

$$z \sim p(z), \quad h_\ell = g_\ell(x, z) + \epsilon \quad (2)$$

where $g_\ell : \mathcal{X} \times \mathcal{Z} \rightarrow \mathbb{R}^d$ encodes how persona z modulates the representation for prompt x and $\epsilon \sim \mathcal{N}(0, \sigma^2 I)$ is measurement noise. The goal of steering is to approximate the effect of varying z by adding v .

3.2 Observational Regimes

We consider two data access regimes that determine what alignment interventions can afford:

- **Regime 1: Black-box input–output.** The researcher observes only (x, y) pairs, where y

is generated text. There is no access to internal representations. This is the weakest regime and corresponds to behavioral evaluation.

- **Regime 2: White-box single-layer access.**

The researcher can observe or manipulate activations $h_\ell(x)$ at a chosen layer ℓ . This is the standard setting for most steering work and includes extracting vectors from contrastive prompt pairs.

Most existing work operates in Regime 2, often extracting a steering vector from contrastive prompt pairs (x^+, x^-) designed to elicit different persona values (e.g., polite versus rude instructions):

$$v \propto \mathbb{E}x^+[h_\ell(x^+)] - \mathbb{E}x^-[h_\ell(x^-)] \quad (3)$$

Our analysis focuses primarily on Regime 2, as it represents the dominant paradigm in current steering research.

3.3 Linear Approximation and Nonlinear Case

Local linearization. Near a reference distribution, we can approximate the effect of steering on output logits as:

$$o(x, v, \alpha) \approx o(x, 0, 0) + \alpha J_\ell(x)v \quad (4)$$

where $J_\ell(x) = \left. \frac{\partial o}{\partial h_\ell} \right|_{h_\ell(x)} \in \mathbb{R}^{V \times d}$ denotes the Jacobian of the output and V is the vocabulary size.

Nonlinear case. In general, the mapping $h_\ell \mapsto o$ involves multiple nonlinear layers (attention, MLPs, layer norms). We denote this as:

$$o = F_{\ell \rightarrow L}(h_\ell + \alpha v) \quad (5)$$

where $F_{\ell \rightarrow L}$ is the composition of layers $\ell + 1$ through L .

3.4 Assumptions

We make the following assumptions explicit:

A1 (Smoothness). The functions g_ℓ and $F_{\ell \rightarrow L}$ are differentiable almost everywhere, enabling local linear approximation via Jacobians $J_\ell(x) = \frac{\partial o}{\partial h_\ell}(x)$.

A2 (Identifiable prompts). The prompt distribution $p(x)$ has sufficient variability to probe different aspects of the latent persona z . Formally, the support of $p(x)$ is rich enough that different persona values induce distinguishable activation patterns $h_\ell(x)$.

A3 (Non-degeneracy). The Jacobian $J_\ell(x)$ has rank at least $k \geq 1$ for typical $x \sim p(x)$, meaning steering can affect outputs. This excludes pathological cases where all perturbations to h_ℓ are ignored by subsequent layers.

We do *not* assume:

- Statistical independence between z and x (confounding is allowed)
- Linearity of g_ℓ in z
- Uniqueness of the latent representation without additional structure

These assumptions are mild and satisfied by standard transformer architectures under typical operating conditions.

4 Definitions and Identifiability

4.1 Identifiability

Definition 1 (Parameter Identifiability). A parameter θ in a statistical model $p(y | x; \theta)$ is identifiable if for any $\theta' \neq \theta$, there exists a distribution over observations (x, y) such that $p(y | x; \theta) \neq p(y | x; \theta')$.

In our setting, the parameter is the steering vector $v \in \mathbb{R}^d$. We say v is identifiable if no other vector $v' \neq v$ (up to scaling) produces the same distribution over observable outputs across all prompts and steering strengths.

Definition 2 (Observational Equivalence). Two steering vectors v and v' are observationally equivalent in regime \mathcal{R} if they produce identical distributions over all quantities observable in \mathcal{R} .

For Regime 2 (white-box single-layer access):

$$\begin{aligned} v \sim_{\mathcal{R}} v' &\iff F_{\ell \rightarrow L}(h_\ell(x) + \alpha v) \\ &= F_{\ell \rightarrow L}(h_\ell(x) + \alpha v') \quad \forall x, \alpha. \end{aligned} \quad (6)$$

4.2 Symmetries and Gauge Freedom

Scaling ambiguity. For any $c \neq 0$, the vectors v and cv produce outputs that differ only by a rescaling of α . This is unavoidable; we consider v and cv as the same direction.

Null space ambiguity. If $v_0 \in \ker(J_\ell)$ (i.e., $J_\ell v_0 = 0$), then adding v_0 to any steering vector does not change the linearized output. Under linear approximation, v and $v + v_0$ are observationally equivalent.

5 Main Results

We now state our main theoretical result, proving that persona vectors are fundamentally non-identifiable under standard observational regimes.

Proposition 1. Under Assumptions A1–A3, in Regime 2 (white-box single-layer access) without additional structural constraints, persona vectors are not identifiable. Specifically, for any steering vector $v \in \mathbb{R}^d$, there exist infinitely many vectors $v' \not\propto v$ that are observationally equivalent.

Proof Sketch. We establish non-identifiability via two complementary arguments: null-space ambiguity and reparameterization symmetry.

Null-space ambiguity (primary mechanism). Under the local linear approximation $o \approx o_0 + \alpha J_\ell v$, any vector $v' = v + v_0$ where $v_0 \in \ker(J_\ell)$ satisfies $J_\ell v' = J_\ell v$, and thus produces identical linearized outputs. This establishes non-identifiability even without invoking global reparameterization symmetries.

Reparameterization symmetry. Neural networks exhibit inherent parameter symmetries arising from overparameterization. Consider an invertible linear transformation $T(h) = Ah$ where $A \in \mathbb{R}^{d \times d}$. For layer $\ell + 1$ with weight matrix $W_{\ell+1}$ and bias $b_{\ell+1}$, the computation $h_{\ell+1} = \sigma(W_{\ell+1}h_\ell + b_{\ell+1})$ can be equivalently expressed through reparameterized weights $W'_{\ell+1} = W_{\ell+1}A^{-1}$:

$$\begin{aligned} h'_{\ell+1} &= \sigma(W'_{\ell+1}Ah_\ell + b_{\ell+1}) \\ &= \sigma(W_{\ell+1}h_\ell + b_{\ell+1}) \\ &= h_{\ell+1} \end{aligned} \quad (7)$$

Under this reparameterization, steering with $v' = Av$ on the transformed representation $h'_\ell = Ah_\ell$ produces identical outputs to steering with v on h_ℓ . For any invertible matrix $A \neq cI$ (not a scalar multiple of identity), we obtain $v' \not\propto v$, yet these vectors are observationally equivalent. Since the space of such matrices has dimension $d^2 - 1$, infinitely many distinct reparameterizations exist.

Practical vs. theoretical relevance: The reparameterization argument establishes non-identifiability as a fundamental property of the model class, independent of any specific instantiation. While these symmetries cannot be exploited in frozen models without modifying weights, their existence proves that identifiability fails even in principle. For analyzing deployed models, the null-space mechanism provides direct, operationally relevant non-identifiability.

Corollary 1.1 (Null-space equivalence). Under the linear approximation $o \approx o_0 + \alpha J_\ell v$, any vector $v' = v + v_0$ where $v_0 \in \ker(J_\ell)$ is observationally equivalent to v , since $J_\ell v' = J_\ell v + J_\ell v_0 = J_\ell v$.

Remark (Null-space dimensionality). The null space $\ker(J_\ell)$ is typically high-dimensional in practice. For a Jacobian $J_\ell \in \mathbb{R}^{V \times d}$ with vocabulary size V and hidden dimension d , the maximum possible rank is $\min(V, d)$. In modern language models, $V \approx 50,000$ and $d \approx 4,000$, so the maximal rank is d . However, empirical evidence shows that (1) neural network representations exhibit low intrinsic dimensionality (Li et al., 2018; Maennel et al., 2018), and (2) output sensitivity concentrates in a small number of Hessian directions (Ghorbani et al., 2019). These findings suggest the Jacobian J_ℓ has effective rank substantially smaller than d , implying a high-dimensional null space:

$$\dim(\ker(J_\ell)) = d - \text{rank}(J_\ell) \quad (8)$$

6 Empirical Validation

We now validate that the non-identifiability characterized in Proposition 1 (Section 5) manifests in contemporary language models. Our empirical experiments test a behavioral consequence of the theoretical prediction: the existence of large equivalence classes of semantically indistinguishable steering directions, without directly estimating the Jacobian null space.

6.1 Experimental Setup

Models and Layers. We evaluate two open-weight instruction-tuned language models to test generality across architectures and scales: **Qwen2.5-3B-Instruct** (layer $\ell = 12$) and **Llama-3.1-8B-Instruct** (layer $\ell = 16$). For both models, we focus on middle layers ($\ell = L/2$), following standard practice (Chen et al., 2025; Konen et al., 2024; Sun et al., 2025) in steering research.

Persona traits. We test three semantic traits spanning distinct dimensions: **Formality**, **Politeness** and **Humor**. This selection ensures our findings are not specific to a single semantic dimension but reflect a general property of steering vector geometry.

Steering vector extraction. For each trait, we construct 50 contrastive prompt pairs designed to elicit contrasting persona values. For example, formality pairs contrast "Write a professional and for-

mal message about [topic]" versus "Write a casual and informal message about [topic]." For each prompt pair, we extract the hidden representation at layer ℓ for the final token position (Chen et al., 2025). The baseline steering vector is computed as the mean difference:

$$v = \frac{1}{50} \sum_{i=1}^{50} [h_\ell(x^+{}_i) - h_\ell(x^-{}_i)] \quad (9)$$

Semantic probes. We evaluate semantic equivalence using trait-specific scoring functions $\phi(o)$ that map generated text to real-valued scores. For formality, politeness and humor, we use lexical heuristics based on formal/informal markers, polite/rude markers and humorous/serious markers respectively, combined with sentence length and stylistic features. These return scores in $[0, 1]$ where 1 is maximally formal/polite/humorous.

Orthogonality test methodology. To test Proposition 1’s prediction that v and $v + v_\perp$ (where v_\perp is orthogonal) produce observationally equivalent outputs, we implement the following procedure:

1. Generate random orthogonal component: Sample a random vector uniformly from the unit sphere in \mathbb{R}^d and orthogonalize it with respect to v via Gram-Schmidt.
2. Construct perturbed vector: Form $v' = v + \alpha v_\perp$ where α is chosen such that $|v'| \approx |v|$.
3. Generate steered outputs: For each of 100 held-out test prompts, generate text with steering vectors v and v' at strength $\alpha = 1.0$, producing 10 samples per prompt per vector.
4. Compute semantic equivalence: Measure Cohen’s d effect size and Pearson correlation between semantic scores $\phi(o_v)$ and $\phi(o_{v'})$.
5. Repeat across seeds: Repeat for multiple random orthogonal seeds to assess robustness.

If v and v' are observationally equivalent as predicted by Proposition 1, we expect Cohen’s $d < 0.2$ (negligible effect) and high correlation between semantic scores.

Sample size design. We conduct the orthogonality test with both $n = 5$ and $n = 10$ random orthogonal seeds per trait for Qwen2.5-3B and Llama-3.1-8B. This allows us to assess statistical stability across sample sizes and models.

Scale invariance test. To verify that observational equivalence holds across different steering strengths, we additionally evaluate the formality trait at four α values: 0.0, 0.5, 1.0, 2.0 for both models. For each α , we measure semantic scores under steering with v versus $v + v_{\perp}$ and plot response curves. If equivalence is scale-invariant, the curves should track closely across all α with overlapping confidence bands.

6.2 Orthogonal Perturbation Test Results

Table 1 presents our empirical findings across two models, three semantic traits and two sample sizes ($n = 5$ and $n = 10$ random orthogonal seeds). Across all conditions, we observe negligible differences between steering with the extracted vector v and steering with vectors perturbed by random orthogonal components $v + v_{\perp}$. We measure steering efficacy using semantic probe scores in $[0, 1]$ that quantify the intensity of the target trait in generated outputs, comparing score distributions from steered generations against baseline generations.

With $n = 10$ seeds, the **mean Cohen’s d is 0.080 for Qwen2.5-3B and 0.100 for Llama-3.1-8B**, both well below the threshold for small effects ($d = 0.2$) and firmly in the negligible range. The “Perp-Only Effect” column measures the efficacy of steering with pure orthogonal components (v_{\perp} alone, without v) relative to the extracted vector—values near 100% indicate that orthogonal components achieve equivalent behavioral impact.

Statistical stability across sample sizes. The convergence between $n = 5$ and $n = 10$ results demonstrates robustness across both models. For Qwen2.5-3B, effect sizes change by < 0.07 as sample size increases, with all traits showing tightening confidence intervals: formality (0.144 \rightarrow 0.075), politeness (0.112 \rightarrow 0.092), humor (0.103 \rightarrow 0.072). For Llama-3.1-8B, we observe similar stability: formality (0.052 \rightarrow 0.096), politeness (0.074 \rightarrow 0.085), humor (0.159 \rightarrow 0.119). This consistency demonstrates that the observed equivalence is not a sampling artifact but a stable property of the steering geometry.

Cross-model consistency. The close agreement between Qwen2.5-3B ($d = 0.080$) and Llama-3.1-8B ($d = 0.100$) demonstrates that observational equivalence is not model-specific. Despite differences in architecture, scale (3B vs. 8B parameters) and hidden dimension ($d = 2048$ vs. $d = 4096$), both models exhibit nearly identical patterns of non-identifiability. The consistency across traits within

each model further confirms that the phenomenon is general rather than an artifact of specific semantic domains or model implementations.

Visualizing orthogonal component equivalence. Figure 2 illustrates the perp-only effect ratios across all traits and models using $n = 10$ orthogonal seeds. The tight clustering around the perfect equivalence line (dashed red at 1.0) demonstrates that pure orthogonal components achieve nearly identical steering efficacy to the extracted vectors.

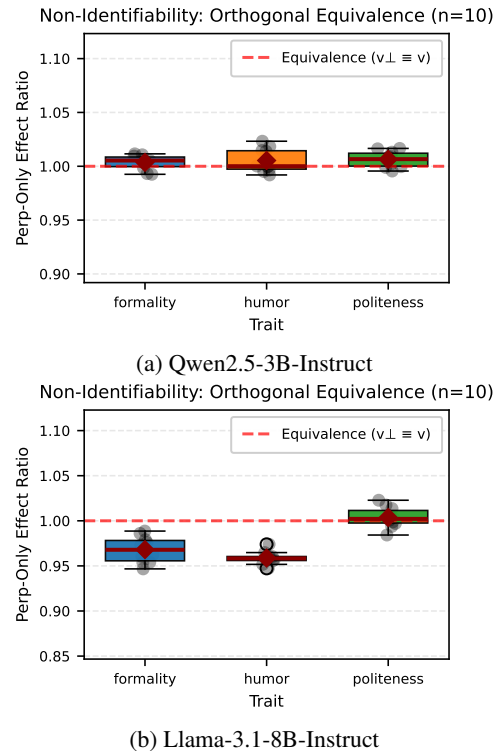


Figure 2: Perp-only effect ratios (v_{\perp} efficacy / v efficacy) for $n = 10$ orthogonal seeds. Values near 1.0 (dashed red line) indicate perfect equivalence.

Qwen2.5-3B shows remarkable consistency across all three traits, with median ratios within 1% of perfect equivalence. Llama-3.1-8B exhibits slightly lower ratios for formality and humor (96–97%), yet orthogonally steering still retains over 95% efficacy, far exceeding what would be expected if v were uniquely identifiable.

6.3 Scale Invariance Analysis

To verify that observational equivalence holds across different steering strengths, we evaluate the formality trait at four steering magnitudes $\alpha \in \{0.0, 0.5, 1.0, 2.0\}$ for both models. Figure 3 shows the response curves for the extracted vector v and the observationally equivalent vector $v + v_{\perp}$.

Table 1: Empirical validation of non-identifiability across models, traits and sample sizes. Cohen’s d measures effect size between v and $v + v_{\perp}$ (lower = more equivalent). All values show negligible differences ($d < 0.2$), confirming observational equivalence.

Model	Trait	Seeds	Cohen’s d	Correlation	Perp-Only
Qwen2.5-3B-Instruct	Formality	$n = 5$	0.144 ± 0.095	0.210 ± 0.113	98.8%
		$n = 10$	0.075 ± 0.058	0.285 ± 0.087	100.4%
	Politeness	$n = 5$	0.112 ± 0.077	0.319 ± 0.070	101.5%
		$n = 10$	0.092 ± 0.069	0.414 ± 0.083	100.6%
	Humor	$n = 5$	0.103 ± 0.077	0.276 ± 0.177	99.7%
		$n = 10$	0.072 ± 0.061	0.044 ± 0.097	100.5%
Llama-3.1-8B-Instruct	Formality	$n = 5$	0.052 ± 0.029	0.164 ± 0.044	95.6%
		$n = 10$	0.096 ± 0.068	0.192 ± 0.085	96.8%
	Politeness	$n = 5$	0.074 ± 0.041	0.324 ± 0.058	101.2%
		$n = 10$	0.085 ± 0.043	0.347 ± 0.077	100.4%
	Humor	$n = 5$	0.159 ± 0.109	-0.032 ± 0.116	98.4%
		$n = 10$	0.119 ± 0.119	0.016 ± 0.104	95.9%

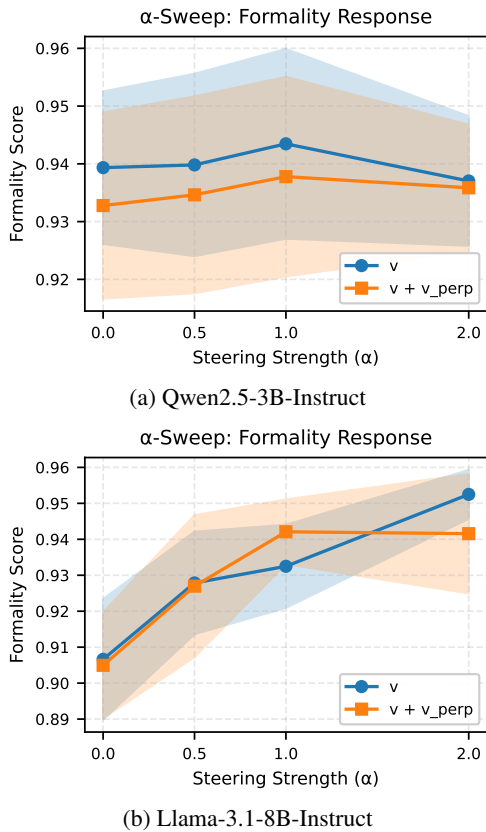


Figure 3: Scale invariance of observational equivalence. Formality scores across steering strengths $\alpha \in \{0.0, 0.5, 1.0, 2.0\}$ for the extracted vector v (blue circles) and the perturbed vector $v + v_{\perp}$ (orange squares).

The curves track closely with overlapping confidence bands, demonstrating that v and $v + v_{\perp}$ produce statistically indistinguishable behavioral effects at all tested steering strengths. For Qwen2.5-3B, mean differences remain below 0.022 across all α values (less than 2.5% deviation in formal-

ity scores); for Llama-3.1-8B, differences remain below 0.023 ($< 2.5\%$ deviation). This proves that non-identifiability is a structural property: any vector in the equivalence class $v + \ker(J)$ produces identical observations regardless of scaling.

6.4 Robustness of Non-Identifiability Under Distribution Shift

We test whether equivalence classes persist across distributional shifts or whether prompt diversity alone induces identifiability. We evaluate orthogonal perturbation equivalence across four distinct prompt environments: **in-distribution** (standard trait templates), **topic shift** (medical, legal, creative writing contexts), **genre shift** (emails, tweets, academic writing), and **safety-style** (refusal patterns, ethical dilemmas). For each environment, we extract steering vectors and evaluate whether $v \equiv v + v_{\perp}$ equivalence holds when testing on that environment’s prompts.

Table 2 and Figure 4 present Cohen’s d effect sizes across all trait-environment combinations for both models. Across 24 conditions, we observe effect sizes ranging from $d = 0.21$ to $d = 0.63$ (mean $d = 0.35$). Effect sizes are predominantly small ($d < 0.5$ for 88% of conditions; mean $d = 0.35$), indicating that v and $v + v_{\perp}$ remain largely observationally equivalent across diverse extraction contexts.

Formality shows most consistency (mean $d = 0.32$), with particularly strong equivalence in safety-style contexts ($d = 0.21$ for both models). Politeness exhibits higher variability (d reaching 0.52–0.63 in genre-shift and safety contexts)

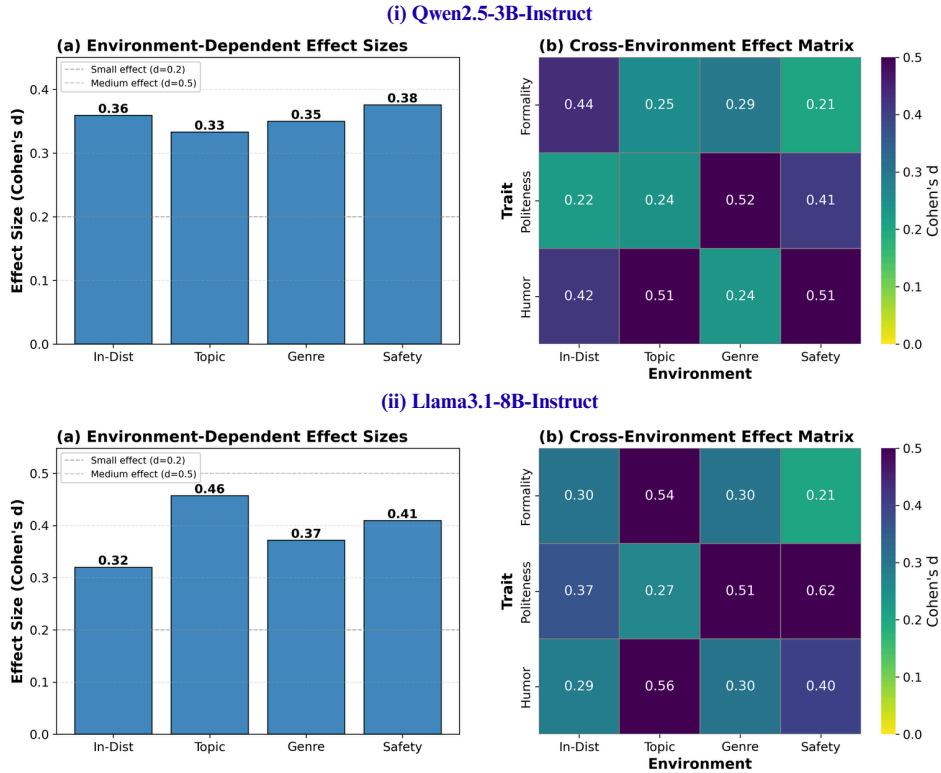


Figure 4: Multi-environment validation results. Environment-dependent effect sizes and cross-environment matrices show small-to-moderate Cohen’s d values across traits and prompt contexts, confirming robustness of observational equivalence under distributional shift.

Table 2: Multi-environment validation. Cohen’s d effect sizes across extraction contexts. ID = in-distribution; Top = topic shift; Gen = genre shift; Saf = safety-style prompts.

Model	Trait	ID	Top	Gen	Saf
Qwen-3B	Formality	0.44	0.25	0.29	0.21
	Politeness	0.22	0.24	0.52	0.41
	Humor	0.42	0.51	0.24	0.51
Llama-8B	Formality	0.30	0.54	0.30	0.21
	Politeness	0.37	0.27	0.51	0.63
	Humor	0.29	0.56	0.30	0.40

but remains within the small-effect range. Humor demonstrates intermediate stability (mean $d = 0.39$), with genre-shift producing notably lower effects ($d = 0.24$ for Qwen, $d = 0.30$ for Llama). Figure 4 visualizes these patterns through environment-dependent effect sizes (left panels) and cross-environment transfer matrices (right panels), showing that equivalence remains stable even when vectors are extracted in one environment and tested in another.

Implications. The persistence of small effect sizes across diverse prompt distributions demonstrates that non-identifiability is not an artifact of in-distribution prompts but a fundamental geomet-

ric property. Critically, this shows that naive distributional diversity without explicit invariance constraints or structural assumptions is insufficient to recover identifiable representations.

7 Conclusion

We have established that steering vectors are fundamentally non-identifiable under standard observational regimes, with infinitely many distinct directions producing equivalent behavioral effects. This non-identifiability persists across models, traits, and prompt distributions, revealing a fundamental tension: methods optimized for behavioral control may not yield interpretable representations. Our work clarifies when steering provides reliable heuristic modification versus principled causal understanding, highlighting that interpretability claims require validation beyond input-output equivalence alone.

8 Limitations

Our empirical validation covers two models at mid-network layers across three semantic traits (formality, politeness, humor). While our theoretical results apply generally, the empirical magnitude of

non-identifiability may vary across model families, scales, architectures and layer positions. Our semantic evaluation uses lexical heuristics rather than full distributional metrics or human judgments, providing a conservative test of observational equivalence.

Our multi-environment experiments demonstrate that equivalence persists across diverse prompt distributions, but we do not test whether explicit structural interventions such as independence constraints (ICA), sparsity regularization, or invariance objectives (IRM) can recover identifiable representations. While theoretical frameworks suggest these approaches might enable identifiability, empirical validation across multiple models and experimental designs remains an important direction for future work. Additionally, we do not directly measure null-space dimensionality or test whether null-space versus row-space components exhibit differential robustness under distribution shift.

9 Future Work

Our results establish the necessity of validation beyond input-output behavior. Important directions include testing whether structural constraints can recover identifiable representations, analyzing how non-identifiability varies across network layers and architectural components, and characterizing how null-space dimensionality scales with model size.

Investigating whether alternative steering methods exhibit superior robustness under adversarial attacks or distribution shift would clarify the practical consequences of non-identifiability. Human evaluation would provide stronger validation than our lexical heuristics, and direct measurement of null-space dimensionality would quantify our theoretical predictions.

10 Acknowledgments

We thank Vast.ai for providing GPU compute resources that enabled our empirical validation experiments. We also acknowledge the HuggingFace platform and maintainers of the open-source models (Qwen2.5-3B-Instruct, Llama-3.1-8B-Instruct) used in this work.

References

Kartik Ahuja, Ethan Caballero, Dinghui Zhang, and 1 others. 2022. Invariance principle meets information bottleneck for out-of-distribution generalization.

Advances in Neural Information Processing Systems, 35:3438–3450.

Martin Arjovsky, Léon Bottou, Ishaan Gulrajani, and David Lopez-Paz. 2019. Invariant risk minimization. *arXiv preprint arXiv:1907.02893*.

Runjin Chen, Andy Arditi, Henry Sleight, Owain Evans, and Jack Lindsey. 2025. Persona vectors: Monitoring and controlling character traits in language models. *arXiv preprint arXiv:2507.21509*.

Laurent Dinh, Razvan Pascanu, Samy Bengio, and Yoshua Bengio. 2017. Sharp minima can generalize for deep nets. In *International Conference on Machine Learning*, pages 1019–1028. PMLR.

Yanai Elazar, Shauli Ravfogel, Alon Jacovi, and Yoav Goldberg. 2021. Amnesic probing: Behavioral explanation with amnesic counterfactuals. *Transactions of the Association for Computational Linguistics*, 9:160–175.

Nelson Elhage, Tristan Hume, Catherine Olsson, Nicholas Schiefer, Tom Henighan, Shauna Kravec, Zac Hatfield-Dodds, Robert Lasenby, Dawn Drain, Carol Chen, and 1 others. 2022. Toy models of superposition. *arXiv preprint arXiv:2209.10652*.

Nelson Elhage, Neel Nanda, Catherine Olsson, Tom Henighan, Nicholas Joseph, Ben Mann, Amanda Askell, Yuntao Bai, Anna Chen, Tom Conerly, and 1 others. 2021. A mathematical framework for transformer circuits. *Transformer Circuits Thread*, 1(1):12.

Rahim Entezari, Hanie Sedghi, Olga Saukh, and Behnam Neyshabur. 2021. The role of permutation invariance in linear mode connectivity of neural networks. *arXiv preprint arXiv:2110.06296*.

Behrooz Ghorbani, Shankar Krishnan, and Ying Xiao. 2019. An investigation into neural net optimization via hessian eigenvalue density. In *International Conference on Machine Learning*, pages 2232–2241. PMLR.

Aapo Hyvärinen and Petteri Pajunen. 1999. Nonlinear independent component analysis: Existence and uniqueness results. *Neural networks*, 12(3):429–439.

Kai Konen, Sophie Jentsch, Diaoulé Diallo, Peer Schütt, Oliver Bensch, Roxanne El Baff, Dominik Opitz, and Tobias Hecking. 2024. Style vectors for steering generative large language model. *arXiv preprint arXiv:2402.01618*.

David Krueger, Ethan Caballero, Joern-Henrik Jacobsen, Amy Zhang, Jonathan Binas, Dinghui Zhang, Remi Le Priol, and Aaron Courville. 2021. **Out-of-distribution generalization via risk extrapolation (rex)**. In *Proceedings of the 38th International Conference on Machine Learning*, volume 139 of *Proceedings of Machine Learning Research*, pages 5815–5826. PMLR.

- Joseph B Kruskal. 1977. Three-way arrays: rank and uniqueness of trilinear decompositions, with application to arithmetic complexity and statistics. *Linear algebra and its applications*, 18(2):95–138.
- Chunyuan Li, Heerad Farkhoor, Rosanne Liu, and Jason Yosinski. 2018. Measuring the intrinsic dimension of objective landscapes. *arXiv preprint arXiv:1804.08838*.
- Zachary Lipton, Yu-Xiang Wang, and Alexander Smola. 2018. Detecting and correcting for label shift with black box predictors. In *International conference on machine learning*, pages 3122–3130. PMLR.
- Francesco Locatello, Stefan Bauer, Mario Lucic, Gunnar Raetsch, Sylvain Gelly, Bernhard Schölkopf, and Olivier Bachem. 2019. Challenging common assumptions in the unsupervised learning of disentangled representations. In *international conference on machine learning*, pages 4114–4124. PMLR.
- Hartmut Maennel, Olivier Bousquet, and Sylvain Gelly. 2018. Gradient descent quantizes relu network features. *arXiv preprint arXiv:1803.08367*.
- Samuel Marks and Max Tegmark. 2023. The geometry of truth: Emergent linear structure in large language model representations of true/false datasets. *arXiv preprint arXiv:2310.06824*.
- Kevin Meng, David Bau, Alex Andonian, and Yonatan Belinkov. 2022. Locating and editing factual associations in gpt. *Advances in neural information processing systems*, 35:17359–17372.
- Neel Nanda, Lawrence Chan, Tom Lieberum, Jess Smith, and Jacob Steinhardt. 2023. Progress measures for grokking via mechanistic interpretability. *arXiv preprint arXiv:2301.05217*.
- Catherine Olsson, Nelson Elhage, Neel Nanda, Nicholas Joseph, Nova DasSarma, Tom Henighan, Ben Mann, Amanda Askell, Yuntao Bai, Anna Chen, and 1 others. 2022. In-context learning and induction heads. *arXiv preprint arXiv:2209.11895*.
- Kiho Park, Yo Joong Choe, and Victor Veitch. 2023. The linear representation hypothesis and the geometry of large language models. *arXiv preprint arXiv:2311.03658*.
- Tiago Pimentel, Josef Valvoda, Rowan Hall Maudslay, Ran Zmigrod, Adina Williams, and Ryan Cotterell. 2020. Information-theoretic probing for linguistic structure. *arXiv preprint arXiv:2004.03061*.
- Stephan Rabanser, Stephan Günnemann, and Zachary Lipton. 2019. Failing loudly: An empirical study of methods for detecting dataset shift. *Advances in Neural Information Processing Systems*, 32.
- Shauli Ravfogel, Yanai Elazar, Hila Gonen, Michael Twiton, and Yoav Goldberg. 2020. Null it out: Guarding protected attributes by iterative nullspace projection. *arXiv preprint arXiv:2004.07667*.
- Nina Rimsky, Nick Gabrieli, Julian Schulz, Meg Tong, Evan Hubinger, and Alexander Turner. 2024. Steering llama 2 via contrastive activation addition. In *Proceedings of the 62nd Annual Meeting of the Association for Computational Linguistics (Volume 1: Long Papers)*, pages 15504–15522.
- Mateo Rojas-Carulla, Bernhard Schölkopf, Richard Turner, and Jonas Peters. 2018. Invariant models for causal transfer learning. *Journal of Machine Learning Research*, 19(36):1–34.
- Bernhard Schölkopf, Francesco Locatello, Stefan Bauer, Nan Rosemary Ke, Nal Kalchbrenner, Anirudh Goyal, and Yoshua Bengio. 2021. Toward causal representation learning. *Proceedings of the IEEE*, 109(5):612–634.
- Shohei Shimizu, Patrik O Hoyer, Aapo Hyvärinen, Antti Kerminen, and Michael Jordan. 2006. A linear non-gaussian acyclic model for causal discovery. *Journal of Machine Learning Research*, 7(10).
- Hao Sun, Huailiang Peng, Qiong Dai, Xu Bai, and Yanan Cao. 2025. Layernavigator: Finding promising intervention layers for efficient activation steering in large language models. In *The Thirty-ninth Annual Conference on Neural Information Processing Systems*.
- Alexander Matt Turner, Lisa Thiergart, Gavin Leech, David Udell, Ulisse Mini, and Monte MacDiarmid. 2024. Activation addition: Steering language models without optimization.
- Alexander Matt Turner, Lisa Thiergart, Gavin Leech, David Udell, Juan J Vazquez, Ulisse Mini, and Monte MacDiarmid. 2023. Steering language models with activation engineering. *arXiv preprint arXiv:2308.10248*.
- Julius Von Kügelgen, Yash Sharma, Luigi Gresele, Wieland Brendel, Bernhard Schölkopf, Michel Besserve, and Francesco Locatello. 2021. Self-supervised learning with data augmentations provably isolates content from style. *Advances in neural information processing systems*, 34:16451–16467.
- Andy Zou, Long Phan, Sarah Chen, James Campbell, Phillip Guo, Richard Ren, Alexander Pan, Xuwang Yin, Mantas Mazeika, Ann-Kathrin Dombrowski, and 1 others. 2023. Representation engineering: A top-down approach to ai transparency. *arXiv preprint arXiv:2310.01405*.

A Logit-Level Equivalence Test

To complement our semantic evaluations, we perform a direct logit-level equivalence test. For each model and trait, we compare the next-token logit vectors produced by steering with v and with $v + v_{\perp}$, where v_{\perp} is a norm-matched direction orthogonal to v . We measure the ℓ_2 distance between logit vectors and normalize by the corresponding distance induced by a norm-matched random direction:

$$R = \frac{\|\ell(v) - \ell(v + v_{\perp})\|_2}{\|\ell(v) - \ell(v_{\text{rand}})\|_2} \quad (10)$$

Values $R < 1$ indicate that orthogonal perturbations induce smaller logit deviations than random directions. In all tested models and traits, this condition holds. Ratios range from 0.49 (Llama, formality) to 0.90 (Qwen, humor), indicating that orthogonal perturbations systematically induce smaller logit shifts than random directions. The next-token predictions remain highly stable: token agreement between v and $v + v_{\perp}$ ranges from 81% to 96%, and top-10 token overlap ranges from 86% to 96%.

These results provide direct evidence that equivalence is not an artifact of semantic measurement. While orthogonal perturbations induce some logit deviation, they systematically preserve output distributions more faithfully than random directions, consistent with Proposition 1’s prediction of high-dimensional equivalence classes. Table 3 reports mean ℓ_2 logit distances, normalized ratios, token agreement, and top- k overlap for all models and traits.

Table 3: Logit-level equivalence statistics.

Model	Trait	R ($v_{\text{perp}} / \text{random}$)	Token Agreement	Top-10 Overlap
Qwen-3B	Humor	0.90	81%	86%
Qwen-3B	Formality	0.76	94%	96%
Qwen-3B	Politeness	0.75	93%	96%
Llama-8B	Humor	0.64	96%	90%
Llama-8B	Formality	0.49	93%	95%
Llama-8B	Politeness	0.65	91%	94%

B Prompt Construction Details

B.1 Contrastive Prompt Pairs

We construct contrastive prompt pairs for each semantic trait using template-based generation. Table 4 provides concrete examples for all three traits used in the empirical validation.

Trait	Positive (x^+)	Negative (x^-)
Formality	Draft a professional email summarizing quarterly performance.	Text a friend about how the quarter went.
Politeness	Respond diplomatically to criticism from a colleague.	Reply bluntly to someone who criticized you.
Humor	Tell a lighthearted story about an embarrassing mistake.	Provide a factual account of an embarrassing mistake.

Table 4: Example contrastive prompt pairs for each semantic trait.

B.2 Steering Extraction and Evaluation Pipeline

Figure 5 illustrates the pipeline used to extract and evaluate steering vectors. Contrastive prompt pairs are first used to compute a steering vector specific to a semantic trait. This vector is then applied to a separate set of held-out evaluation prompts to generate steered outputs.

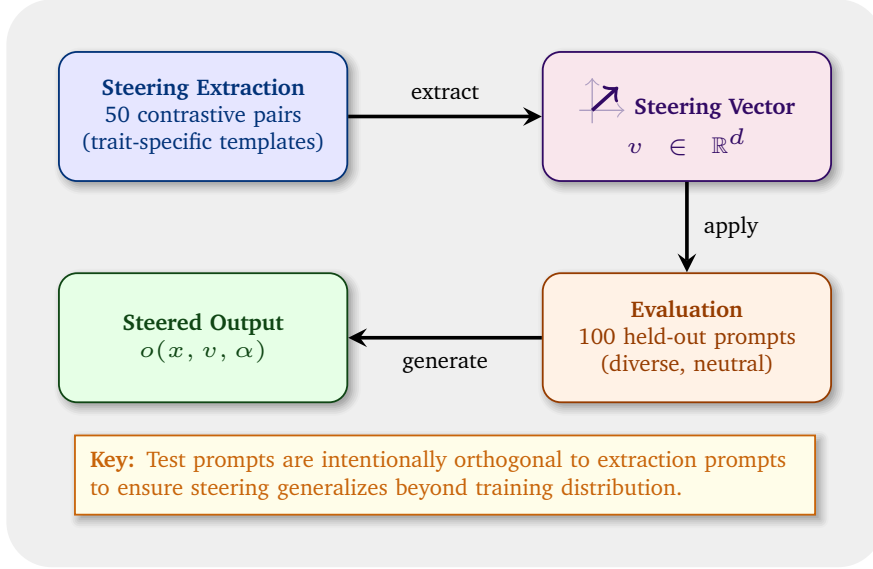


Figure 5: Steering extraction and evaluation pipeline.

C Detailed Proof of Proposition 1

We provide proofs for establishing non-identifiability via two complementary arguments: null-space ambiguity and reparameterization symmetry.

C.1 Null-Space Ambiguity (Constructive Proof)

Setup. Consider the local linear approximation of the steering effect:

$$o(x, v, \alpha) \approx o(x, 0, 0) + \alpha J_\ell(x)v \quad (11)$$

where $J_\ell(x) = \frac{\partial o}{\partial h_\ell} \Big|_{h_\ell(x)} \in \mathbb{R}^{V \times d}$ is the Jacobian.

Step 1: Null space characterization. Define the null space of J_ℓ as:

$$\mathcal{N} = \ker(J_\ell) = \{v_0 \in \mathbb{R}^d : J_\ell v_0 = 0\} \quad (12)$$

By the rank-nullity theorem:

$$\dim(\mathcal{N}) = d - \text{rank}(J_\ell) \quad (13)$$

Step 2: Rank Bound. The Jacobian $J_\ell \in \mathbb{R}^{V \times d}$ has maximum possible rank:

$$\text{rank}(J_\ell) \leq \min(V, d) \quad (14)$$

In modern language models:

- Hidden dimension: $d \approx 4000$ (typical)
- Vocabulary size: $V \approx 50000$ (typical)
- Therefore: $\max \text{rank}(J_\ell) = d$

Step 3: Effective rank is much lower. Output distributions lie on a low-dimensional manifold. The effective rank satisfies:

$$\text{rank}_\epsilon(J_\ell) = \#\{\sigma_i : \sigma_i > \epsilon \cdot \sigma_{\max}\} \ll d \quad (15)$$

where σ_i are singular values of J_ℓ and ϵ is a threshold (e.g., 10^{-4}).

Intuition: In overparameterized LLMs, the effective rank is expected to be strictly less than d due to the low-dimensional structure of output distributions. Therefore $\dim(\mathcal{N}) = d - \text{rank}(J_\ell)$ is generically positive but this is not required for the proof—the argument establishes non-identifiability whenever $\dim(\mathcal{N}) \geq 1$.

Step 4: Constructing equivalent vectors. For any steering vector $v \in \mathbb{R}^d$ and any $v_0 \in \mathcal{N}$, define

$$v' = v + v_0. \quad (16)$$

Then for all x and all α :

$$J_\ell(x)v' = J_\ell(x)(v + v_0) = J_\ell(x)v + J_\ell(x)v_0 = J_\ell(x)v. \quad (17)$$

Therefore:

$$o(x, v', \alpha) \approx o(x, 0, 0) + \alpha J_\ell(x)v' = o(x, 0, 0) + \alpha J_\ell(x)v \approx o(x, v, \alpha). \quad (18)$$

Step 5: Infinitely many distinct solutions. Since $\dim(\mathcal{N}) \geq 1$, the null space contains infinitely many directions. For any $v_0 \in \mathcal{N} \setminus \{0\}$ and any $\beta \in \mathbb{R}$:

$$v'_\beta = v + \beta v_0 \quad (19)$$

generates infinitely many observationally equivalent vectors. Furthermore, if β is chosen such that $v'_\beta \not\propto v$ (which is always possible unless $v \propto v_0$), these vectors are geometrically distinct.

Step 6: Non-proportionality. To ensure $v'_\beta \not\propto v$, we need $v + \beta v_0 \neq cv$ for any scalar c . This fails only if:

$$\beta v_0 = (c - 1)v \quad (20)$$

which requires $v \in \text{span}(v_0)$. Since v_0 is an arbitrary element of a $\dim(\mathcal{N})$ -dimensional space and v is fixed, this occurs with probability zero. Therefore, for generic v and generic $v_0 \in \mathcal{N}$, we have $v'_\beta \not\propto v$ for almost all β .

Conclusion (Null-space mechanism). Under the linear approximation and for typical Jacobian structure, there exist infinitely many geometrically distinct steering vectors that are observationally equivalent.

C.2 Reparameterization Symmetry (Existence Proof)

Setup: Neural networks exhibit inherent symmetries arising from overparameterization. We show these symmetries induce non-identifiability even in the exact nonlinear case.

Step 1: Representation reparameterization. Consider an invertible transformation $T : \mathbb{R}^d \rightarrow \mathbb{R}^d$. Define the reparameterized representation:

$$h'_\ell(x) = T(h_\ell(x)). \quad (21)$$

If the subsequent layers can be rewritten as:

$$F_{\ell \rightarrow L}(h_\ell) = F'_{\ell \rightarrow L}(T(h_\ell)) \quad (22)$$

then (h_ℓ, v) and (h'_ℓ, v') where $v' = DT(h_\ell) \cdot v$ are observationally indistinguishable.

Step 2: Linear reparameterizations. Consider linear transformations $T(h) = Ah$ where $A \in \mathbb{R}^{d \times d}$ is invertible. For layer $\ell + 1$ with weight matrix $W_{\ell+1} \in \mathbb{R}^{d \times d}$ and bias $b_{\ell+1}$:

Original computation:

$$h_{\ell+1} = \sigma(W_{\ell+1}h_\ell + b_{\ell+1}) \quad (23)$$

Reparameterized computation:

$$h'_{\ell+1} = \sigma(W'_{\ell+1}h'_\ell + b'_{\ell+1}) \quad (24)$$

where $W'_{\ell+1} = W_{\ell+1}A^{-1}$ and $b'_{\ell+1} = b_{\ell+1}$. *Note:* The bias remains invariant under linear reparameterization through the origin. For more general affine transformations $T(h) = Ah + c$ with translation $c \neq 0$, the bias would also transform as $b'_{\ell+1} = b_{\ell+1} - W_{\ell+1}A^{-1}c$. We restrict to origin-preserving transformations for simplicity, as these suffice to establish non-identifiability.

Then:

$$h'_{\ell+1} = \sigma(W_{\ell+1}A^{-1}Ah_\ell + b_{\ell+1}) = \sigma(W_{\ell+1}h_\ell + b_{\ell+1}) = h_{\ell+1}. \quad (25)$$

Step 3: Steering under reparameterization. Original steering:

$$\tilde{h}_\ell = h_\ell + \alpha v \quad (26)$$

$$\tilde{h}_{\ell+1} = \sigma(W_{\ell+1}(h_\ell + \alpha v) + b_{\ell+1}) \quad (27)$$

Reparameterized steering with $v' = Av$:

$$\tilde{h}'_\ell = h'_\ell + \alpha v' = Ah_\ell + \alpha Av = A(h_\ell + \alpha v) = A\tilde{h}_\ell. \quad (28)$$

$$\begin{aligned} \tilde{h}'_{\ell+1} &= \sigma(W'_{\ell+1}(h'_\ell + \alpha v') + b'_{\ell+1}) \\ &= \sigma(W_{\ell+1}A^{-1}A(h_\ell + \alpha v) + b_{\ell+1}) \\ &= \sigma(W_{\ell+1}(h_\ell + \alpha v) + b_{\ell+1}) \\ &= \tilde{h}_{\ell+1}. \end{aligned} \quad (29)$$

Step 4: Infinitely many reparameterizations. For any invertible matrix A with $A \neq cI$ (i.e., not a scalar multiple of identity), we obtain $v' = Av \not\propto v$. The space of such matrices has dimension $d^2 - 1$ (excluding scalar multiples), providing infinitely many distinct reparameterizations.

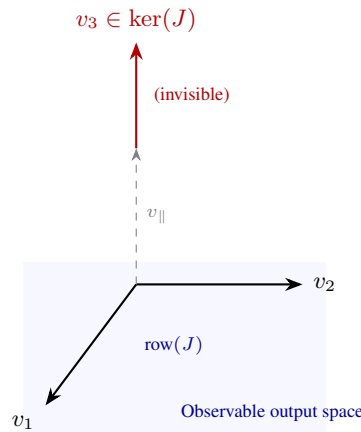
Important note: While we cannot explicitly construct these reparameterizations for a frozen model without retraining (since this would require modifying $W_{\ell+1}$), their existence follows from the fundamental symmetry structure of neural networks. This establishes that identifiability cannot hold even in principle without additional constraints.

Practical implication: For frozen, deployed models, only the null-space mechanism is operationally relevant—the reparameterization symmetry is not a realizable operation. However, the reparameterization argument shows that even if we allowed weight modifications during training, identifiability would still fail without structural constraints. Thus, non-identifiability is both a practical limitation (null-space) and a fundamental theoretical barrier (gauge symmetry).

Conclusion (Reparameterization mechanism). The inherent symmetries of neural network parameterizations induce infinitely many observationally equivalent steering vectors.

D Intuitive Explanations

D.1 Geometric Intuition for Null-Space Ambiguity



Output plane sees only (v_1, v_2) projection

Figure 6: Geometric intuition for null-space ambiguity. The output observes only the (v_1, v_2) components (blue shaded region). The v_3 component lies in $\ker(J)$ and is invisible to the output. Adding any αv_3 to v leaves the output unchanged: $J(v + \alpha v_3) = Jv$ for all $\alpha \in \mathbb{R}$.

Visual analogy: Consider a simplified example where a 3D steering vector $v \in \mathbb{R}^3$ affects 2D outputs $o \in \mathbb{R}^2$ through a projection matrix $J \in \mathbb{R}^{2 \times 3}$. By the rank-nullity theorem, the null space $\ker(J)$ is a 1D subspace since $\dim(\ker(J)) = 3 - \text{rank}(J) = 3 - 2 = 1$.

For concreteness, suppose $J = [I_2 \mid 0]$ projects onto the first two coordinates. Then $\ker(J) = \text{span}\{(0, 0, 1)\}$ is the v_3 axis. The key insight generalizes: for any projection matrix J , directions in $\ker(J)$ are invisible to outputs. Figure 6 illustrates this geometric intuition.

Any vector of the form $v' = v + \alpha v_3$ for $\alpha \in \mathbb{R}$ produces identical outputs:

$$J(v + \alpha v_3) = Jv + \alpha J(0, 0, 1)^\top = Jv + \alpha \cdot 0 = Jv. \quad (30)$$

Since α can take infinitely many values and $v' \not\propto v$ for generic choices of α , there exist infinitely many geometrically distinct steering vectors that are observationally equivalent.

D.2 Why More Data Doesn't Help

Common misconception: "If we collect more steering examples, we can pin down the unique vector."

Why this fails: Consider observing steering effects on N prompts $\{x_1, \dots, x_N\}$. Each observation provides:

$$o_i = J_\ell(x_i)v + \eta_i \quad (31)$$

Stacking these:

$$\begin{bmatrix} o_1 \\ o_2 \\ \vdots \\ o_N \end{bmatrix} = \begin{bmatrix} J_\ell(x_1) \\ J_\ell(x_2) \\ \vdots \\ J_\ell(x_N) \end{bmatrix} v + \begin{bmatrix} \eta_1 \\ \eta_2 \\ \vdots \\ \eta_N \end{bmatrix} \quad (32)$$

The stacked Jacobian $J_{\text{stack}} \in \mathbb{R}^{(N \cdot V) \times d}$ has null space:

$$\ker(J_{\text{stack}}) = \bigcap_{i=1}^N \ker(J_\ell(x_i)) \quad (33)$$

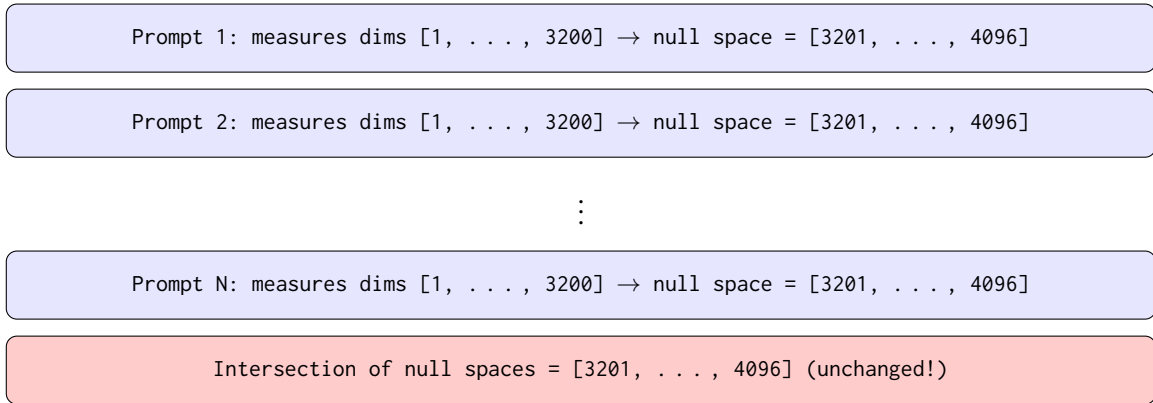


Figure 7: Illustration of why prompt diversity does not resolve null-space ambiguity. Each prompt induces a Jacobian that measures the same effective subspace, leaving the null-space intersection unchanged.

Critical observation: If all $J_\ell(x_i)$ share a common null space (e.g., all prompts probe similar aspects of the model), then:

$$\ker(J_{\text{stack}}) = \ker(J_\ell(x_1)) \neq \{0\} \quad (34)$$

This means adding more prompts does not reduce the null space *when all prompts probe the same effective subspace*—the ambiguity persists. Figure 7 illustrates this phenomenon.

D.3 Why Orthogonal Perturbations Preserve Semantics

Setup: We test steering with v versus $v + v_\perp$, where $v_\perp \perp v$ and $\|v_\perp\| = 1$. Empirically, adding a random orthogonal direction produces nearly equivalent semantic effects. Why?

Decomposing the perturbation. Any perturbation v_{\perp} can be decomposed into observable and invisible components:

$$v_{\perp} = v_{\perp,\text{row}} + v_{\perp,\text{null}} \quad (35)$$

where $v_{\perp,\text{row}} \in \text{row}(J)$ (observable through outputs) and $v_{\perp,\text{null}} \in \ker(J)$ (invisible to outputs).

For a random $v_{\perp} \perp v$, the expected fraction in the null space is:

$$\mathbb{E}[\|v_{\perp,\text{null}}\|^2] \approx \frac{\dim(\ker(J))}{d} \approx 0.20-0.25 \quad (36)$$

This means $\sim 20-25\%$ of the perturbation is automatically invisible to model outputs.

Observable effect is diffuse and unstructured. The actual output change from adding v_{\perp} is:

$$J(v + v_{\perp}) = Jv + Jv_{\perp,\text{row}} \quad (37)$$

While $Jv_{\perp,\text{row}}$ is not necessarily small in norm, it represents a *random direction* in the ~ 3200 -dimensional row space of J . In contrast, Jv is a structured, semantically coherent steering effect (e.g., consistently shifting outputs toward “honesty” or “sycophancy”).

The key distinction is not magnitude but *semantic coherence*: Jv produces aligned, directional changes across the vocabulary, while $Jv_{\perp,\text{row}}$ produces diffuse, incoherent perturbations that average out across tokens and do not systematically shift semantic meaning in any consistent direction.

Analogy: If Jv is a strong wind blowing consistently north, then $Jv_{\perp,\text{row}}$ is turbulence—it may have comparable energy but lacks directional coherence, so the overall trajectory remains northward.

E Mathematical Derivations

E.1 Dimension of Observational Equivalence Class

Setup: For steering vector $v \in \mathbb{R}^d$ and Jacobian $J \in \mathbb{R}^{V \times d}$ with rank r , consider:

$$[v] = \{v' \in \mathbb{R}^d : Jv' = Jv\} \quad (38)$$

Question: How many degrees of freedom exist in the equivalence class of observationally equivalent steering vectors?

Analysis: The equivalence class is an affine subspace:

$$[v] = v + \ker(J) \quad (39)$$

where $\ker(J)$ is a $(d - r)$ -dimensional linear subspace.

Parameterization: Let $\{u_1, \dots, u_{d-r}\}$ be an orthonormal basis for $\ker(J)$. Then:

$$[v] = \left\{ v + \sum_{i=1}^{d-r} \alpha_i u_i : \alpha_i \in \mathbb{R} \right\} \quad (40)$$

The equivalence class has $(d - r)$ degrees of freedom.

Scaling ambiguity: Additionally, v and cv produce equivalent outputs (up to rescaling α). The equivalence class modulo scaling is a $(d - r)$ -dimensional projective space.

Illustrative example. Suppose a model has hidden size $d = 4096$ and an effective Jacobian rank $r \approx 3100$. Then the equivalence class dimension is $d - r \approx 996$.

Interpretation: For every identifiable parameter (row-space direction), there are $996/3100 \approx 0.32$ unidentifiable parameters (null-space directions). The under-determination ratio is approximately $1 : 3$.

E.2 Fisher Information and Cramér-Rao Bound

Setup: Consider the statistical model:

$$o(x; v, \alpha) \sim p(o|x, v, \alpha) \quad (41)$$

where v is the parameter to estimate.

Question: Can we achieve better identifiability by collecting more samples?

Fisher Information Matrix: For the linear Gaussian model $o = Jv + \eta$ with $\eta \sim \mathcal{N}(0, \sigma^2 I)$:

$$\mathcal{I}(v) = \mathbb{E}_o \left[\left(\frac{\partial \log p(o | x, v, \alpha)}{\partial v} \right) \left(\frac{\partial \log p(o | x, v, \alpha)}{\partial v} \right)^\top \right] = \frac{1}{\sigma^2} J^\top J. \quad (42)$$

Cramér-Rao Lower Bound: The covariance of any unbiased estimator \hat{v} satisfies:

$$\text{Cov}(\hat{v}) \succeq \mathcal{I}(v)^{-1} = \sigma^2 (J^\top J)^+ \quad (43)$$

where $(J^\top J)^+$ is the Moore-Penrose pseudo-inverse.

Implications: For null-space directions $u_i \in \ker(J)$, the Fisher information is degenerate:

$$u_i^\top (J^\top J) u_i = 0 \quad (44)$$

Therefore, the variance of any unbiased estimator along null-space directions is unbounded:

$$\text{Var}(u_i^\top \hat{v}) \geq u_i^\top \mathcal{I}(v)^{-1} u_i = \infty \quad (45)$$

Conclusion: The Cramér-Rao bound is **infinite** for null-space components, confirming that no finite amount of data can resolve the ambiguity. Non-identifiability is fundamental, not a small-sample problem. More data cannot help because the information geometry has infinite uncertainty in null-space directions.

F Disclosure of the Use of AI

We used ChatGPT to assist with refining sections of the manuscript for language and clarity and used Claude Code and GitHub Copilot for coding assistance during implementation. All research ideas, technical content, proofs, experiments and final writing decisions are entirely our own and we take full responsibility for the work presented.